Optical Manipulation of Atoms and Molecules Using Structured Light

Mohamed Babiker* and David L. Andrews†
* *Department of Physics, University of York, Heslington, York, United Kingdom*
† *School of Chemical Sciences, University of East Anglia, Norwich, United Kingdom*

The interaction of atoms and molecules with structured light, specifically laser light endowed with the property of orbital angular momentum, such as Laguerre-Gaussian light, is discussed. The primary effects of interest here are the influence of the light on the gross motion of atoms and molecules and the possibilities this motion provides for particle manipulation in cooling, heating and trapping experiments. It turns out that, in addition to the possibility of modifying translational motion, suitably structured light can facilitate the manipulation of rotational motion. The latter possibility arises from a light-induced torque that is directly attributable to the orbital angular momentum property of the light. We outline the physics responsible for these effects and consider applications to typical cases in which atoms and ions are subject to near resonant Laguerre-Gaussian beams, leading to characteristic trajectories and eventual trapping in specific regions. Details are given for optical molasses configurations based on twisted light beams arranged in one-, two- and three-dimensional counter-propagating pairs. We extend consideration to the case of liquid crystals, subject to Laguerre-Gaussian light tuned far off-resonance, and show how this leads to the twisting of the directors in the liquid crystal, coinciding with the intensity distribution of the light.

1. Introduction

Optomechanical forces have a long history. The operation of the eighteenth century Crookes radiometer (the familiar rotating propeller in an evacuated bulb) is a popular demonstration of light producing a mechanical force, through a mechanism well known to have its origins in thermal effects. The validity of direct radiation pressure as a mechanical principle was also well understood in that century, and was first experimentally verified using a Nichols radiometer in 1901. Following the development of the laser in 1960, the possibilities for practical utilisation of optomechanical forces to manipulate small particles came newly to the fore, largely owing to the pioneering work of Ashkin about ten years later [1]. Here another principle was established, namely that motion can be produced by forces associated with spatial inhomogeneity in an optical beam. This field evolved very rapidly and by the mid-eighties it had led to the invention of optical tweezers, a technique which has since become a mainstream tool for the optical trapping and manipulation of a diverse range of particles.

For optical manipulation, the mechanisms that are most prominent in any specific system are primarily dictated by the size of the target particles. The particle size, in turn, determines the nature of the physical system in which such effects can be observed; the scale of size for optical tweezers and allied methods runs up to a significant fraction of the beam width. Microscopic particles such as cells and polymer beads represent optically controllable particles at this higher limit of size [2-4]. To offset gravitational forces, such materials are most conveniently studied in liquid suspension, and in such cases the particle position and motion are controllable by various means including intensity gradients (optical tweezing of individual particles at a laser focus, or for large numbers of particles in holographically generated traps) and multiple-scattering (optical binding). Together, such methods represent a branch of optical technology that has already found extensive applications in the fields of medicine, sensors and micromechanical devices.

At the opposite extreme, the lower end of the size scale, most such methods are clearly unusable. Individual atoms and small molecules do not present sufficient cross-section to respond differentially, across their own dimensions, to wavelength-scale variations in intensity, nor are they so readily localizable. In the condensed phase, the optical manipulation of particles smaller than 100 nm becomes problematic because of Brownian motion. In the gas phase, laser cooling schemes such as the configuration known as optical molasses, based on

momentum exchange and exploiting Doppler shift to its own ultimate demise, allow the optical generation of traps within which further optical manipulation can be achieved. This science of cold atoms [5-9] has of course recently developed into another burgeoning area of study, the generation and control of Bose-Einstein condensates [10]. In such systems the responsive motion of individual atoms or molecules, or of the whole assembly in the Bose-Einstein case, is determined by an optically generated potential well.

There is a growing recognition of the potential for distinctively nanoscale mechanisms and applications of optomechanical force. The range of activity in this area has recently seen a huge increase, with the latest technological advances leading to new methods of applying optical forces, and the creation of exquisite new beam structures for laser light. This is a subject that now covers a broad and exciting forefront of optical technology. Its focus includes not only nanoscale applications of well developed optical tweezer techniques; it also accommodates topics ranging from cold atom manipulation to optically driven fluidics. In this area, theory and experiment have a particularly vigorous dynamic: theory is constantly informing and suggesting new experiments, while experimental results challenge and invite new theory.

Against this background, the theoretical and technological developments that have led to the production of structured laser light introduce another tier of possibilities associated with orbital angular momentum (OAM) content [11-15]. For the studies to be discussed in this review, the most decisive advance has been the achievement of optical beams with phase-imprinted wavefronts, of which helically twisted Laguerre-Gaussian beams are the most widely studied example (see Fig. 1). While spin angular momentum is one of the best known properties of the photon, most obviously manifest in circular polarisations, recognition has emerged that light beams with a helical wave-front display other kinds of angular momentum, now generally called orbital. This new radiation is often described as a twisted beam or optical vortex, and the torque it exerts an optical spanner. Specifically, if such a beam has an integer number l twists within its wavelength, each photon conveys an orbital angular momentum of $\hbar l$, distinct from any spin angular momentum. Such beams, which are now readily producible in the laboratory, generate optical forces and torques with no counterpart in conventional optics. Already it has been shown that the exploitation of such beams for atomic and molecular manipulation can lead to a variety of lattice structures, clusters and rings [16-18].

In the following, we describe the general principles, and we give the key equations. We also exhibit some of the results that have emerged from studies of optically trapped atoms, and molecules in the quasi-static environment of a liquid crystal [19]. First, we begin with a brief overview of the context of the engagement of light possessing orbital angular momentum with atoms and molecules.

2. Twisted light

Maxwell's theory predicts that a light beam carries both energy and momentum but, until relatively recently, the angular momentum property of light was predominantly understood to refer to the spin angular momentum associated with wave polarisation. The orbital component was only formally defined in Maxwell's theory, and was rarely discussed in an experimental context. The first experiment on optical angular momentum was carried out by Beth [24], but this only concerned circularly polarised light and so it dealt only with the spin component. Related work on the spin optical angular momentum was carried out by P.J. Allen [21], Simon et al. [22] and Bretenaker and Le Floch [23].

The development of lasers as sources of coherent light beams has enabled the production of various modes that can collectively be described as twisted light. This is because such light beams possess an orbital angular momentum arising from their non-uniform spatial distribution. Of particular interest in this context are the Laguerre-Gaussian modes which are characterised by helical wavefront structures involving a number of intertwined helices, as shown schematically in Fig. 1.

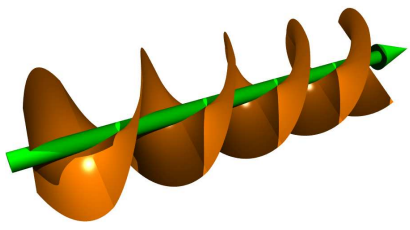

FIG. 1: Schematic wavefront structure of a Laguerre-Gaussian light beam with three intertwined helices.

The production of Laguerre-Gaussian light beams involves the use of an ordinary laser beam with planar wavefronts in the form of rectangularly symmetric Hermite-Gaussian modes, characterised by two integer indices m and n. A Laguerre-Gaussian (LG) mode will conveniently emerge on passing Hermite-Gaussian light through a pre-designed computer generated hologram. Such a LG mode is characterised by two indices: an azimuthal integer index l, representing the number of intertwined helices and a radial integer index p, representing the number of radial nodes. We will use the notation LG_{lp} to donate a Laguerre-Gaussian mode of indices (l, p). When both l and p are zero, we get a $(0, 0)$ mode as an ordinary Gaussian distribution that carries no angular momentum and has no radial nodes. For $l \neq 0$ and $p = 0$ we have the so-called doughnut (donut) modes, which exhibit ring shaped intensity distributions, as shown Fig.2 for the cases $l = 1$ and $l = 3$. Figure 2 also shows the case of two-rings mode arising when $l = 1, p = 1$. A photon of an LG_{lp} beam carries a well defined orbital angular momentum equal to $l\hbar$. This was first shown by Allen et al. using the paraxial approximation [20]. Within the paraxial approximation [24] we have for the electric field vector of a Laguerre-Gaussian beam travelling in the +z-direction and polarised principally in the x direction

$$\tilde{\boldsymbol{\mathcal{E}}}_{klp}(\mathbf{R}) = i\omega \left(u_{klp}\hat{\mathbf{x}} + \frac{i}{k}\frac{\partial u_{klp}}{\partial x}\hat{\mathbf{z}} \right) e^{ikz} \qquad (1)$$

The function u_{klp} can be written in cylindrical coordinates $\mathbf{R} = (r, \phi, z)$ as follows

$$u_{klp}(r, \phi, z) = \frac{C}{(1 + z^2/z_R^2)^{1/2}} \left(\frac{r\sqrt{2}}{w(z)} \right)^l \cdot L_p^l \left(\frac{2r^2}{w^2(z)} \right) e^{-\left(r^2/w^2(z)\right)} e^{i\Theta_{klp}(r,\phi,z)} \qquad (2)$$

where

$$\Theta_{klp}(r, \phi, z) = \frac{ikr^2 z}{2(z^2 + z_R^2)} + l\phi + (2p + l + 1)\tan^{-1}(z/z_R) \quad (3)$$

where z_R is the Rayleigh range and $w^2(z) = 2(z^2 + z_R^2)/kz_R$ is the beam width at distance z from the beam waist (at $z = 0$) and C is a normalisation factor.

A characteristic feature of all modes possessing orbital angular momentum is the phase factor $e^{il\phi}$.

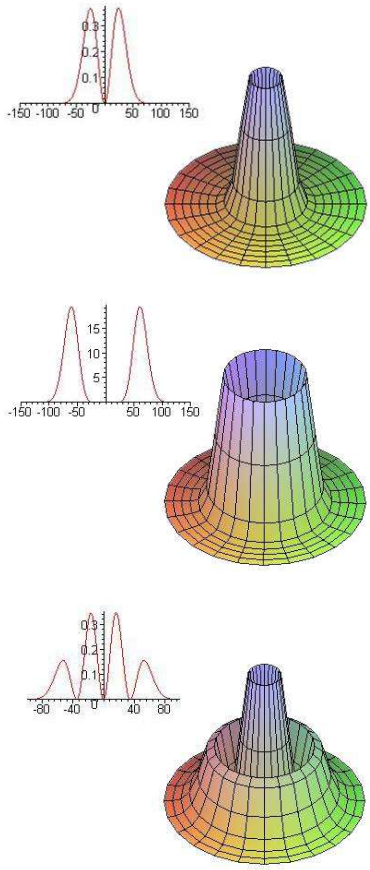

FIG. 2: The intensity distributions of modes, respectively, for $\mathrm{LG}_{1,0}$ (donut mode), $\mathrm{LG}_{3,0}$ (donut mode) and $\mathrm{LG}_{1,1}$ (two-ring). These radial intensity distributions are at the waist plane $z = 0$. The insets exhibit graphically the corresponding radial intensity distributions with radial distance in units of wavelength. The functional forms of LG modes are given below.

This term will be shown here to be responsible for all rotational effects when Laguerre-Gaussian light interacts with atoms and molecules

3. Atoms and molecules in LG beams - brief overview

The literature dealing with study of the engagement of light endowed with orbital angular momentum with atoms and molecules is relatively sparse in comparison with that involving optical manipulation of the larger particles [6] mentioned above, such as biological cells and polymer beads. Most published works on atoms and molecules are con-

cerned with theoretical studies, but there are also a few experimental studies.

The possibility that orbital angular momentum effects can influence matter at the atomic and molecular level was first mentioned as a speculation in pioneering work by Allen et al. [24]. This was followed by a number of theoretical investigations [25-29] that led to the prediction of the light-induced torque [25], the azimuthal Doppler shift [26] and a number of studies on the motion of atoms and ions in Laguerre-Gaussian beams, including optical molasses in one, two and three dimensions [27-29]. The role of photon spin when considered in the same context as OAM was clarified [28]. This led to the identification of a spin-orbit term and a contribution involving l-s coupling in the azimuthal force due to circularly polarised Laguerre-Gaussian light. More recent work concentrated on trapping in dark regions of the beam profile, indicating that under such circumstances the trapped atoms would experience diminished heating effects [30]. Studies dealing with the selection rules governing the interaction of light with the internal and external degrees of freedom were undertaken by van Enk [31] and Babiker et al. [32], while Juzeliunas et al. identified novel features in the interactions of Bose-Einstein condensates [33,34]. As interest in the subject has grown, many other groups have also engaged with the issues surrounding the effects of OAM on atoms and molecules [35-40].

The first experimental study involving atoms interacting with orbital angular momentum of light was that by Tobosa and Petrov [41] in which they demonstrated the transfer of OAM from the beam to cold caesium atoms. Other studies have dealt with the channelling of atoms in material structures possessing cylindrical symmetry, where the optical modes are distinguished by orbital angular momentum features. Theoretical studies [42,43] have shown that, in such structures, the channelling of atoms involves light torques similar to those produced by free space Laguerre-Gaussian beams - which have also been employed as atom guides [44-49]. In the molecular context particular interest has focused on liquid crystals, despite their complexity, since their distinctive combination of anisotropic local structure and relatively labile orientational motion is directly amenable to optical interrogation. The effects of OAM on liquid crystals have been studied recently by Piccarillo and co-workers [50,51] and a subsequent analysis employing the dielectric model of the nematic liquid crystal has been reported by Carter et al. [19].

4. Transfer of OAM to atoms and molecules

For both structured and unstructured light, most optical processes involve electric dipole interactions with the radiation fields, this type of interaction generally being the strongest form of coupling. Depending on the specific process, the dipolar interactions entailed may invoke either static or transition moments. In connection with the interactions of structured light - twisted beams in particular - distinctive issues revolve around the possible involvement of other electric and magnetic multipoles. One issue concerns the possibility that the left- or right-handed character of a twisted beam (i.e. the handedness of its helical wavefront surface) might engage differentially with fluids comprising chiral molecules, according to the molecular handedness. This hinges on the form of the electromagnetic coupling because, in such media, chiral discrimination requires electronic transitions to be simultaneously allowed by multipoles of opposite parity: this is a problem addressed in Chapter 15.

Berry [52] showed theoretically that the orbital angular momentum is an intrinsic property of all types of azimuthal phase-bearing light. If so, then it could be argued that in its interaction with an atom or a molecule, orbital angular momentum should be exchanged in an optical transition, just as spin angular momentum is exchanged in a radiative transition. Another question arises in connection with the multipolar interactions of twisted light. This concerns the fact that the photon orbital angular momentum can engage in electric quadrupole and higher electric multipole interactions, and it is necessary to consider whether this might introduce modified selection rules for electronic transitions. These matters have been explored by an explicit analysis [14], which concluded that the exchange of OAM occurs in the electric dipole approximation and couples only the centre of mass to the light beam. The internal degrees of freedom associated with the 'electronic' motion are not involved in any OAM exchange with the light beam to this leading order. It is only in the next order, namely in an electric quadrupole transition, that an exchange involving the light, the centre of mass and the internal degrees of freedom can be realised. One unit of OAM is exchanged between the light and the internal dynamics, so that the light beam possesses $(l \pm 1)\hbar$ units of OAM and the centre of mass motion gains ± 1 units. These conclusions suggest that no experiments can detect OAM exchange between Laguerre-Gaussian light

and molecular systems through changes involving electric dipole transitions. The analysis confirms the fact that OAM effects are manifest primarily in the centre mass motion by the imposition of additional forces and associated torques. The study of these additional forces is best carried out by a extending the formalism of Doppler cooling and trapping to the case of light possessing OAM, as we discuss next.

5. Doppler forces and torques

It has long been known that the Doppler effect responsible for broadening atomic transitions can be exploited for laser cooling. On irradiating an atomic gas with a laser beam detuned to the red of an absorption frequency, only a subset of the atoms - those that experience a compensating (blue) Doppler shift due to motion towards the light source - can absorb the light. The decay of the resulting excited state releases a photon in a random direction. Due to the extremely short lifetime usually associated with the excited state, this is a process that can recur with great rapidity, and the net effect over a series of absorption and emission cycles is that such atoms experience a net imparted momentum against their direction of travel, slowing them down. For the self-selected group of atoms within the laser beam profile this loss of translational energy signifies cooling, to the extent that such a term can meaningfully be applied to a non-equilibrium system. With two counter-propagating beams the velocities of the fastest atoms in each direction can be reduced, and as the laser frequency is gradually increased the breadth of the initially Maxwellian velocity distribution becomes increasingly narrow. Transverse motions can be controlled by the addition of further counter-propagating beams, with each pair of sources in a mutually orthogonal configuration; this is the essence of optical molasses.

The significant features introduced by the use of structured light possessing orbital angular momentum are: (i) there is, in addition to translational effects, a light-induced torque which causes a rotational motion of the atoms about the beam axis and; (ii) there are regions of maximum and minimum intensities in the beam cross-section. The forces and torque are, in general, time-dependent as well as position-dependent. As we discuss below, the full space- and time-dependence of the motion is, in general, characterised by a transient regime, followed by a steady state regime after a sufficiently large time has elapsed from the instant in which the beam is switched on (typically for elapsed times much larger than the characteristic timescale of the problem).

5.1. Essential formalism

Consider an atom or a molecule for which the gross motion is that of the centre of mass and the internal dynamics is modelled in terms of a two-level atom. In the presence of a laser field, the total Hamiltonian for the whole system is

$$H = \hbar\omega a^\dagger a + \frac{\mathbf{P}^2}{2M} + \hbar\omega_0 \pi^\dagger \pi - i\hbar\left[\tilde{\pi}^\dagger f(\mathbf{R}) - h.c.\right] \tag{4}$$

where $\tilde{\pi}$ and $f(\mathbf{R})$ are given by

$$\tilde{\pi} = \pi \mathrm{e}^{i\omega t}; \quad f(\mathbf{R}) = (\boldsymbol{\mu}_{12}\cdot\hat{\boldsymbol{\epsilon}})\alpha\mathcal{F}_{klp}(\mathbf{R})\mathrm{e}^{i\Theta_{klp}(\mathbf{R})}/\hbar \tag{5}$$

Here π and $\pi^\dagger$ are the ladder operators for the two-level system; $\mathbf{P}$ is the centre-of-mass momentum operator with M the total mass and ω_0 the dipole transition frequency. The operators a and $a^\dagger$ are the annihilation and creation operators of the laser light and ω is its frequency. In the classical limit, appropriate for the case of a coherent beam, the a and $a^\dagger$ operators become c-numbers involving the parameter α such that

$$a(t) \to \alpha \mathrm{e}^{-i\omega t}; \qquad a^\dagger(t) \to \alpha^* \mathrm{e}^{i\omega t}. \tag{6}$$

The last term in eq(4) is the interaction Hamiltonian coupling the laser light to the two-level system in the electric dipole and rotating wave approximations, evaluated at the centre of mass position vector $\mathbf{R}$. The coupling function $f(\mathbf{R})$ in Eq.(5) involves $\boldsymbol{\mu}_{12}$, the transition dipole matrix element of the atom interacting with a Laguerre-Gaussian light mode characterised by $\hat{\boldsymbol{\epsilon}}$, the mode polarisation vector, the mode amplitude function, $\mathcal{F}_{klp}(\mathbf{R})$ and phase $\Theta_{klp}(\mathbf{R})$, given by

$$\begin{aligned}\mathcal{F}_{klp}(\mathbf{R}) &= \mathcal{F}_{k00}\frac{N_{lp}}{(1+z^2/z_R^2)^{1/2}}\left(\frac{\sqrt{2}r}{w(z)}\right)^{|l|} \\ &\quad \cdot L_p^{|l|}\left(\frac{2r^2}{w^2(z)}\right)\mathrm{e}^{-r^2/w^2(z)}, \qquad (7)\\ \Theta_{klp}(\mathbf{R}) &= \frac{kr^2 z}{2(z^2+z_R^2)} + l\phi + \\ &\quad 2p+l+1)\tan^{-1}(z/z_R) + kz, \qquad (8)\end{aligned}$$

Here $\mathcal{F}_{k00}$ may be identified as the amplitude for a plane wave propagating along the z-axis with wavevector k; the coefficient $N_{lp} = \sqrt{p!/(|l|+p!)}$ is a normalisation constant; $w(z)$ is a characteristic width of the beam at axial coordinate z and is explicitly given by $w^2(z) = 2(z^2 + z_R^2)/kz_R$, where z_R is the Rayleigh range. The LG mode indices l and p determine the field intensity distribution and are such that $l\hbar$ is the orbital angular momentum content carried by each quantum.

We now assume the position $\mathbf{R}$ and the momentum operator $\mathbf{P}$ of the atomic centre of mass should take their average values $\mathbf{r}$ and $\mathbf{P}_0 = M\mathbf{V}$, where $\mathbf{V}$ is the centre of mass velocity. Thus we are treating the atom gross motion classically, while its internal motion continues to be treated quantum mechanically. This treatment is justified provided that the spread in the atomic wavepacket is much smaller than the wavelength of the light, and that the recoil energy is much smaller than the linewidth. The system density matrix can then be written as

$$\rho_S = \delta(\mathbf{R} - \mathbf{r})\delta(\mathbf{P} - M\mathbf{V})\rho(t), \tag{9}$$

where $\rho(t)$ is the internal density matrix, which follows the time evolution

$$\frac{d\rho}{dt} = -\frac{i}{\hbar}[H, \rho] + \mathcal{R}\rho, \tag{10}$$

and where the term $\mathcal{R}\rho$ represents the relaxation processes in the two-level system. The optical Bloch equations governing the evolution of the density matrix elements can be written as follows

$$\begin{bmatrix} \dot{\hat{\rho}}_{21}(t) \\ \dot{\hat{\rho}}_{12}(t) \\ \dot{\rho}_{22}(t) \end{bmatrix} = \begin{bmatrix} -(\Gamma_2 - i\Delta) & 0 & 2f(\mathbf{r}) \\ 0 & -(\Gamma_2 + i\Delta) & 2f^*(\mathbf{r}) \\ -f^*(\mathbf{r}) & -f(\mathbf{r}) & -\Gamma_1 \end{bmatrix} \cdot \begin{bmatrix} \hat{\rho}_{21}(t) \\ \hat{\rho}_{12}(t) \\ \rho_{22}(t) \end{bmatrix} + \begin{bmatrix} -f(\mathbf{r}) \\ -f^*(\mathbf{r}) \\ 0 \end{bmatrix} \tag{11}$$

Here the relaxation processes are assumed to be characterised by an inelastic collision rate, Γ_1, and an elastic collision one, Γ_2. The effective, velocity-dependent, detuning Δ is given by $\Delta = \Delta_0 - \boldsymbol{\nabla}\Theta.\mathbf{V}$ and we have set $\hat{\rho} = \tilde{\rho}\exp(-it\mathbf{V}\cdot\boldsymbol{\nabla}\Theta)$. We have also made use of the relation $\rho_{11}(t) + \rho_{22}(t) = 1$.

The average force due to the light acting on the centre of mass is the expectation value of the trace of $-\rho\boldsymbol{\nabla}H$,

$$\langle \mathbf{F} \rangle = -\langle tr(\rho\boldsymbol{\nabla}H) \rangle \tag{12}$$

The total force can be written as the sum of two types of force, a dissipative force $\langle \mathbf{F}_{diss} \rangle$ and a dipole force $\langle \mathbf{F}_{dipole} \rangle$, and these are related to the density matrix elements as follows

$$\langle \mathbf{F}_{diss}(\mathbf{R}, t) \rangle = -\hbar\boldsymbol{\nabla}\Theta(\hat{\rho}_{21}^* f(\mathbf{r}) + \hat{\rho}_{21} f^*(\mathbf{r})) \tag{13}$$

$$\langle \mathbf{F}_{dipole}(\mathbf{R}, t) \rangle = i\hbar\frac{\boldsymbol{\nabla}\Omega}{\Omega}(\hat{\rho}_{21}^* f(\mathbf{r}) - \hat{\rho}_{21} f^*(\mathbf{r})). \tag{14}$$

Here we have introduced the position dependent Rabi frequency $\Omega(\mathbf{R})$, defined as

$$\hbar\Omega(\mathbf{R}) = |(\boldsymbol{\mu}_{12}\cdot\hat{\boldsymbol{\epsilon}})\alpha\mathcal{F}(\mathbf{R})|; \qquad f(\mathbf{R}) = \Omega(\mathbf{R})\mathrm{e}^{i\Theta(\mathbf{R})} \tag{15}$$

Clearly all quantities depend on the mode type and implicitly carry the labels klp.

The centre of mass dynamics is determined by Newton's second law, written in the form

$$M\frac{d^2\mathbf{R}}{dt^2} = \langle \mathbf{F}(t) \rangle \tag{16}$$

where $\langle \mathbf{F}(t) \rangle$ is the total average force. Since this differential equation is second order in time, values of the position vector components $\mathbf{R}(0)$ and initial velocity vector components $\mathbf{V}(0)$ should be stated as initial conditions. The main outcome of solving Eq.(16) is a complete determination of the trajectory function $\mathbf{R}(t)$, along with $\mathbf{V}(t) = \dot{\mathbf{R}}(t)$. Furthermore, as will become apparent, the development furnishes important information about the evolution of the light-induced torque.

5.2. Transient dynamics

The transient effects are most prominent for transitions with a long excited state lifetime. Rare-earth ions provide such a context; we consider an Eu^{3+} ion which has M= 25.17×10^{-26} kg and for its ${}^5D_0 \rightarrow {}^7D_1$ transition $\lambda = 614$ nm and $\Gamma = 1111$ Hz. We focus on the $l = 1$, $p = 0$ Laguerre-Gaussian mode and assume the laser intensity to be $I = 10^5$ W cm^{-2}, and the beam waist $w_0 = 35\lambda$. The transient regime can be explored for three special cases, namely (a) exact resonance; (b) strong collisions and (c) intense field. For the latter case we shall assume the higher intensity $I = 10^8$ W cm^{-2}. Evaluations have been carried out for a period $t_{max} \approx 5\Gamma^{-1} \approx 4.5$ ms, which is sufficiently long to exhibit effects both for the transient regime and the steady state.

The results are shown in Fig.3 for the cases of strong collisions. The atom follows a characteristic path with an axial motion superimposed on an in-plane motion. The in-plane motion is seen to be in

the form of loops in the shape of petals. It is in this characteristic motion that the effects of the optical torque are evident. A similar trajectory arises in

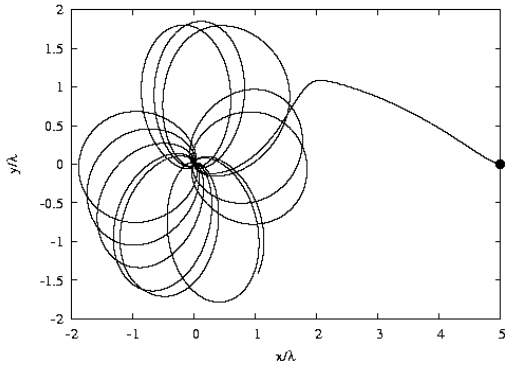

FIG. 3: The path in the x-y-plane of an Eu^{3+} ion subject to an $LG_{1,0}$ mode in the case of strong collisions. The initial position is represented by a dot. Other parameters used for the generation of this figure are given in the text.

the case of an intense external field, as shown in Fig. 4, but here it is seen that there are many more loops due to the atom gaining kinetic energy with a larger force and torque. Fig. 5 explores the initial stages of the trajectory before the second petal is formed. In the case of exact resonance, Fig. 6, there is no dipole force acting on the atom and so no radial force, due to the zero-detuning. The atomic radial position is constant.

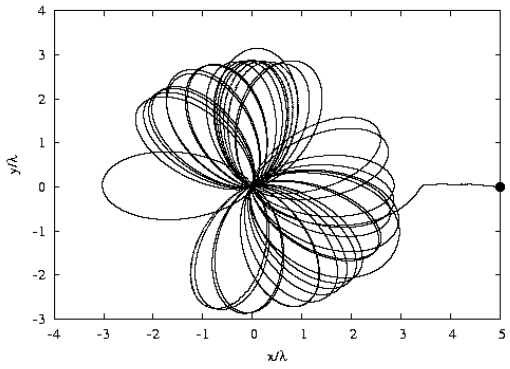

FIG. 4: As in Fig. 3, but for the case of a strong external field, as described in the text.

The time-dependent torque is defined as

$$\boldsymbol{\mathcal{T}}(t) = \mathbf{r}(t) \times \langle \mathbf{F}(t) \rangle \tag{17}$$

The evolution of this torque can be determined along with the corresponding trajectories. The

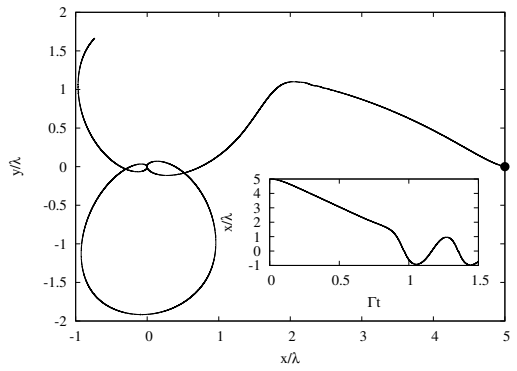

FIG. 5: The initial stages of the trajectories shown in Figs. 3 and 4, exhibiting the initiation of the first petal-like loop. Inset: variation of the x-component of the position with time.

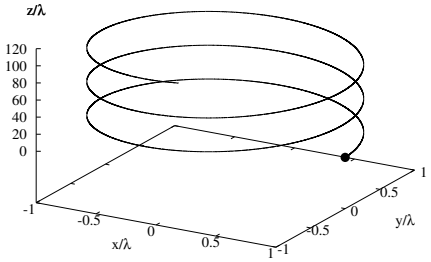

FIG. 6: The path of an Eu^{3+} ion subject to a $LG_{1,0}$ in the case of exact resonance. Other parameters are the same as those in Figs. 3 and 4.

torque experienced by the Eu^{3+} ion for the case of strong collisions is displayed in Fig. 7. It is evident from Fig. 7 that once the beam is switched on, there is an abrupt increase in the magnitude of the torque, which then oscillates and rapidly decays towards a steady state value. Furthermore the evolution exhibits a collapse and revival pattern, with each cycle corresponding to a loop in the trajectory. The peak of the torque corresponds to the outer tip of the loop, and the collapse corresponds to the points near the beam axis. The sudden jumps in the torque are real events arising from the change in the direction of motion as the atom is repelled from regions of extremum field intensity values.

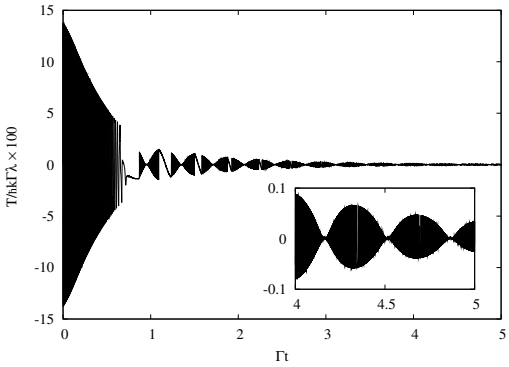

FIG. 7: The variation of the (axial) light-induced torque acting on the Eu^{3+} ion subject to a $LG_{1,0}$ in the case of strong collisions. The detuning $\Delta_0 = 500\Gamma$ and the initial radial position is $r = 5\lambda$

5.3. Steady state dynamics

The formal expressions for the steady state forces can be deduced by taking the limit $t \to \infty$, or the time derivatives in the optical Bloch equations set equal to zero. In the steady state, where $\Gamma t \gg 1$ (where Γ is the de-excitation rate of the upper state of the atomic transition), the total force on a two-level atom exhibits position-dependence and is naturally divisible into two terms. Restoring the explicit reference to a specific Laguerre-Gaussian mode, the steady state force on a moving atom due to a single beam propagating along the positive z axis is written

$$\langle \mathbf{F} \rangle_{klp} = \langle \mathbf{F}_{diss} \rangle_{klp} + \langle \mathbf{F}_{dipole} \rangle_{klp} \tag{18}$$

where $\langle \mathbf{F}_{diss} \rangle_{klp}$ is the dissipative force

$$\langle \mathbf{F}_{diss}(\mathbf{R}, \mathbf{V}) \rangle_{klp} = 2\hbar\Gamma\Omega^2_{klp}(\mathbf{R}) \cdot \left(\frac{\boldsymbol{\nabla}\Theta_{klp}(\mathbf{R})}{\Delta^2_{klp}(\mathbf{R}, \mathbf{V}) + 2\Omega^2_{klp}(\mathbf{R}) + \Gamma^2} \right) \tag{19}$$

and $\langle \mathbf{F}_{dipole}(\mathbf{R}, \mathbf{V}) \rangle_{klp}$ is the dipole force

$$\langle \mathbf{F}_{dipole}(\mathbf{R}, \mathbf{V}) \rangle_{klp} = -2\hbar\Omega_{klp}(\mathbf{R})\boldsymbol{\nabla}\Omega_{klp} \cdot \left(\frac{\Delta_{klp}(\mathbf{R}, \mathbf{V})}{\Delta^2_{klp}(\mathbf{R}, \mathbf{V}) + 2\Omega^2_{klp}(\mathbf{R}) + \Gamma^2} \right) \tag{20}$$

The effective detuning $\Delta_{klp}(\mathbf{R}, \mathbf{V})$ is now both position- and velocity-dependent;

$$\Delta_{klp}(\mathbf{R}, \mathbf{V}) = \Delta_0 - \mathbf{V}.\boldsymbol{\nabla}\Theta_{klp}(\mathbf{R}, \mathbf{V}) \tag{21}$$

The dissipative force is due to absorption followed by spontaneous emission of light by the atom, while the dipole force is seen to be proportional to the gradient of the Rabi frequency. Both types of force feature prominently in atom cooling and trapping, with the dissipative force creating a net a frictional force in optical molasses, and the dipole force trapping the atom in regions of extremum field intensity.

The inference that a light induced torque is automatically created in this context can be confirmed by examining at the velocity-independent forces. For $\mathbf{V} = 0$ and for $z << z_R$ we have

$$\left\langle \mathbf{F}^0_{diss}(\mathbf{R}) \right\rangle_{klp} = \frac{2\hbar\Gamma\Omega^2_{klp}(\mathbf{R})}{\Delta^2_0 + 2\Omega^2_{klp}(\mathbf{R}) + \Gamma^2} \left[k\hat{\mathbf{z}} + \frac{l}{r}\hat{\phi} \right] \tag{22}$$

There are thus two components of force: an axial component and an azimuthal component. The latter has a non-vanishing moment about the axis, i.e. a torque given by

$$\boldsymbol{\mathcal{T}} = \frac{2\hbar\Gamma\Omega^2_{klp}(\mathbf{R})}{\Delta^2_0 + 2\Omega^2_{klp}(\mathbf{R}) + \Gamma^2} l\hat{\mathbf{z}} \tag{23}$$

In the saturation limit, where $\Omega >> \Delta_0$ and $\Omega >> \Gamma$ we have

$$\boldsymbol{\mathcal{T}} \approx \hbar l\Gamma\hat{\mathbf{z}} \tag{24}$$

This simple form of the light-induced torque was first pointed out by Babiker et al. [25]. In general, the

torque is velocity- and position-dependent, and therefore changes along the path of the atom.

5.4. Dipole potential

The velocity-independent dipole force can be derived from the dipole potential

$$\langle U(\mathbf{R}) \rangle_{klp} = \frac{\hbar\Delta_0}{2} \ln \left[1 + \frac{2\Omega^2_{klp}(\mathbf{R})}{\Delta^2_0 + \Gamma^2} \right] \tag{25}$$

such that $\left\langle \mathbf{F}^0_{dipole} \right\rangle_{klp} = -\boldsymbol{\nabla}\langle U(\mathbf{R}) \rangle_{klp}$. This potential would trap atoms in the high intensity regions of the beam for $\Delta_0 < 0$ (red-detuning). For blue detuning, $\Delta_0 > 0$, the trapping would be in the dark regions of the field. For example, consider the LG mode for which $l = 1$, $p = 0$. On the plane of the beam waist $z = 0$, the potential minimum occurs at $r = r_0 = w_0/\sqrt{2}$. For a beam propagating along the z axis the locus of the potential

minimum is a circle in the xy plane given by

$$x^2 + y^2 = r_0^2 \tag{26}$$

Expanding $\langle U(\mathbf{R})\rangle_{k10}$ about r_0 we have

$$\langle U\rangle_{k10} \approx U_0 + \frac{1}{2}\Lambda_{k10}(r - r_0)^2 \tag{27}$$

where $|U_0|$ is the potential depth given by

$$|U_0| = \frac{1}{2}\hbar|\Delta_0| \ln\left[1 + \frac{2\Omega_{k10}^2(r_0)}{\Delta_0^2 + \Gamma^2}\right] \tag{28}$$

and Λ_{k10} is an elastic constant given by

$$\Lambda_{k10} = \frac{4\hbar|\Delta_0|}{\Delta_0^2 + 2e^{-1}\Omega_{k00}^2 + \Gamma^2}\left(\frac{e^{-1}\Omega_{k00}^2}{w_0^2}\right) \tag{29}$$

An atom of mass M, trapped if its energy is less than $|U_0|$, will exhibit a vibrational motion about $r = r_0$ of angular frequency approximately equal to $\{\Lambda_{k10}/M\}^{1/2}$.

6. The Doppler shift

The force expressions contain the effective detuning Δ_{klp} defined by

$$\Delta_{klp} = \omega - \omega_0 - \boldsymbol{\nabla}\Theta_{klp}.\mathbf{V}; \tag{30}$$

this can be written as

$$\Delta_{klp} = \omega - \omega_0 - \delta \tag{31}$$

where δ is an effective Doppler shift associated with the beam. On substituting for $\Theta(\mathbf{R})$ we obtain for δ

$$\begin{aligned}\delta &= \left(\frac{krz}{z^2 + z_R^2}\right)V_r + \frac{lV_\phi}{r} \\ &+ \left\{\frac{kr^2}{2(z^2 + z_R^2)}\left[1 - \frac{2z^2}{z^2 + z_R^2}\right]\right. \\ &\left. + \frac{(2p + l + 1)z_R}{z^2 + z_R^2} + k\right\}V_z\end{aligned} \tag{32}$$

where V_r, V_ϕ and V_z are the velocity components in cylindrical coordinates. The Doppler shift comprises four types of contribution: an axial term, a contribution due to the Guoy phase, a curvature term and an azimuthal contribution, so that

$$\delta = \delta_{axial} + \delta_{Guoy} + \delta_{curve} + \delta_{azimuth} \tag{33}$$

The axial term corresponds to a Doppler shift due to a plane wave travelling along the beam axis

$$\delta_{axial} = kV_z \tag{34}$$

This would be the largest shift if the atom has a substantial axial velocity component. The shift associated with the Guoy phase is

$$\delta_{Gouy} = \left(\frac{(2p + l + 1)z_R}{z^2 + z_R^2}\right)V_z \tag{35}$$

Since typically $z_R >> w_0$, the Guoy shift is normally negligibly small. The shift arising from the beam curvature is

$$\begin{aligned}\delta_{curve} &= \left(\frac{krz}{z^2 + z_R^2}\right)V_r \\ &+ \frac{kr^2}{2(z^2 + z_R^2)}\left[1 - \frac{2z^2}{z^2 + z_R^2}\right]V_z\end{aligned} \tag{36}$$

This is due to beam spreading in the radial and axial directions and arises from the curvature of the wavefront. It could be observable under appropriate conditions. The azimuthal Doppler shift is

$$\delta_{azimuth} = \frac{lV_\phi}{r} \tag{37}$$

This shift is directly proportional to the orbital angular momentum quantum number l of the Laguerre-Gaussian mode and is inversely proportional to the radial coordinate of the atom. It is just one of a number of effects directly attributable to orbital angular momentum content of the light. The Doppler term involving the gradient of the phase is also responsible for the radiation forces generating atomic trajectories, as we now discuss.

6.1. Trajectories

Newton's second law determines the form of the atom dynamics, subject to initial conditions. The solutions lead to the trajectory $\mathbf{R}(t)$ and they also determine the evolution of other variables of the system. Unfortunately, $\mathbf{R}(t)$ cannot, in general, be determined analytically and it is necessary to proceed using numerical analysis. It is easy to check that the trajectories for two cases in which a Mg^+ ion is subject to single separate beams differing only in the sign of l will only display a reversal of the direction of rotation. This is consistent with the existence of the light-induced torque.

6.2. Multiple Beams

Doppler cooling manifests itself in the so-called optical molasses configurations in one, two and three

dimensions. For beams endowed with OAM a description of optical molasses requires the specification of individual field distributions referred to the laboratory coordinate system. We therefore need to apply multiple coordinate transformations with reference to the original Cartesian axes. The total force acting on the atom is the vector sum of individual forces in a given configuration of light beams.

For a light beam of frequency ω, axial wavevector k and quantum numbers l and p coupled to an atom or an ion at a general position vector $\mathbf{R} = (r, \phi, z)$ in cylindrical coordinates, the phase $\Theta_{klp}(\mathbf{R})$ and the Rabi frequency $\Omega_{klp}(\mathbf{R})$ can be taken as follows

$$\Theta_{klp} = l\phi + kz \tag{38}$$

and

$$\Omega_{klp}(\mathbf{R}) \approx \Omega_0 \left(\frac{r\sqrt{2}}{w_0}\right)^{|l|} \exp(-r^2/w_0^2) L_p^{|l|}\left(\frac{2r^2}{w_0^2}\right) \tag{39}$$

These expressions are applicable for a Laguerre-Gaussian beam in the limit $z \ll z_R$, where z_R is the Rayleigh range; also setting $w(z) = w_0$, i.e. ignoring all beam curvature effects.

The total forces acting on the atomic centre of mass moving with velocity $\mathbf{V} = \dot{\mathbf{R}}$ are given above in the steady state, but with the approximate phase $\Theta_{klp}(\mathbf{R})$ and Rabi frequency $\Omega_{klp}(\mathbf{R})$, as in Eqs.(38) and (39). These are given in cylindrical polar coordinates, with the beams propagation parallel to the z-axis. However, in order to consider multiple beams, it is convenient to begin by expressing the position dependence in the Rabi frequency and phase in Cartesian coordinates $\mathbf{R} = (x, y, z)$, simply by the substitutions $r = \sqrt{x^2 + y^2}$ and $\phi = \arctan(y/x)$. A beam propagating in an arbitrary direction is determined by applying two successive transformations. The first transformation is a rotation of the beam about the y-axis by an angle θ and the second is a subsequent rotation about the x axis by an angle ψ. This signifies to the following overall coordinate transformation

$$x \rightarrow x'\cos(\theta)x + \sin(\theta)z \tag{40}$$

$$y \rightarrow y' = -\sin(\theta)\sin(\psi)x + \cos(\psi)y + \cos(\theta)\sin(\psi)z \tag{41}$$

$$z \rightarrow z' - \sin(\theta)\cos(\psi)x - \sin(\psi)y + \cos(\theta)\cos(\psi)z \tag{42}$$

By suitable choice of the angles θ and ψ we obtain the force distribution due to a twisted light beam propagating in any direction. In this manner, we are able to consider geometrical arrangements involving counter-propagating beams (especially those corresponding to one-, two- and three-dimensional optical molasses configurations), for beams possessing OAM.

We concentrate on the case of optical molasses of magnesium ions Mg^+ with a transition of frequency ω_0 corresponding to the transition wavelength $\lambda = 280.1$ nm and transition rate $\Gamma = 2.7 \times 10^8\ \mathrm{s}^{-1}$. The Mg^+ mass $M = 4.0 \times 10^{-26}$ kg. We consider red-detuned light to induce trapping in areas of high intensity, $\Delta_0 = -\Gamma$ and $w_0 = 35\lambda$. The equation of motion for the Mg^+ ion is now

$$M\frac{d^2}{dt^2}\mathbf{R}(t) = \sum_i \langle \mathbf{F}_i \rangle \tag{43}$$

where the sum is taken over individual (total) force contributions from each beam present. In the one-dimensional molasses configuration, a pair of counter-propagating beams is set up along the z axis. The specification of the force due to the beam propagating in the negative z-direction is given by Eqs.(40), (41) and (42) with $\theta = \pi$ and $\psi = 0$. Figure 8 shows the trajectory of the Mg^+ ion with $l_1 = -l_2 = 1$ and $p_1 = p_2 = 0$. The initial radial position is $r = 10\lambda$ and the initial velocity is $\mathbf{V}(0) = 5\mathrm{ms}^{-1}\hat{\mathbf{z}}$. The motion is for a time duration equal to $2 \times 10^5\Gamma^{-1}$. It is clear that the atom

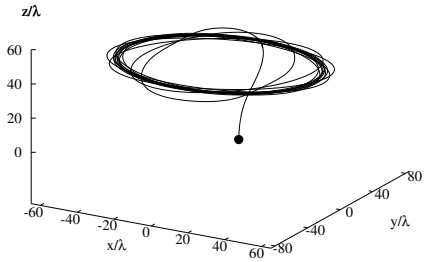

FIG. 8: Path of a Mg^+ ion in the one-dimensional twisted optical molasses created by two counter-propagating Laguerre-Gaussian beans with $l_1 = -l_2 = 1$ and $p_1 = p_2 = 0$ propagating along the z-axis. The initial velocity is $\mathbf{v} = 5\hat{\mathbf{z}}$ ms^{-1}

is slowed down to a halt in the z-direction, while in its motion in the x-y plane it is attracted to the region of high beam intensity at approximately $r_0 > w_0/\sqrt{2}$. The long-time motion is a uniform

circular motion, as can be deduced from Fig. 9 , which exhibits the corresponding evolution of the velocity components. Once the Mg^+ ion is trapped

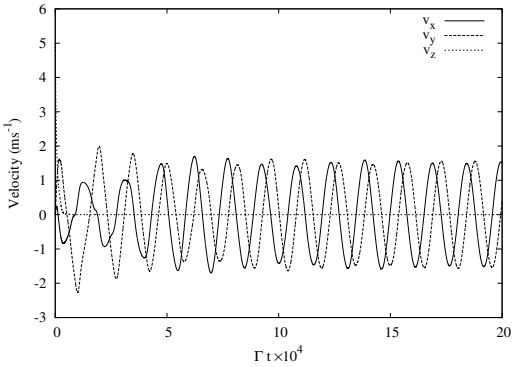

FIG. 9: Evolution of the three velocity components of the Mg^+ ion in the one-dimensional optical molasses of Fig. 8. The axial component of the velocity rapidly approaches zero, consistent with Doppler cooling, while the in-plane components v_x and v_y show a convergence towards uniform circular motion.

axially, it continues to rotates clockwise about the axis, subject to a torque which, in the saturation limit, is given by $|\langle \boldsymbol{\mathcal{T}} \rangle| \approx l_1\hbar\Gamma - l_2\hbar\Gamma = 2\hbar\Gamma$. The motion of the ion gives rise to an electric current equal to $e/\tau \equiv ev_s/2\pi r_0$. With v_s of about 2 ms^{-1} and $r_0 \approx w_0 = 35\lambda$ we have an ionic current of the order of a femtoAmp if a single ion is involved. It is significant that the current scales with the number of trapped ions; obviously a million or so ions can produce a current on the nA scale.

6.3. Two- and three-dimensional molasses

We now introduce a second pair of counter-propagating beams along the x axis and one pair could be characterised by a different width w_0'. The total force is now the vector sum of individual forces from the four beams. The specifications of three of the beams is made with the help of the transformation equations (40)-(42). The trajectories of two Mg^+ ions positioned at different initial points, each having an initial velocity of $v_z = 5\mathrm{ms}^{-1}$, are shown in Fig. 10, where each of the four beams has an azimuthal index, $l = 1$, and radial index, $p = 0$. Since by choice of l values in this case, the total torque arising from either pair of beams is zero; each ion ends up at a specific fixed point, where it remains essentially motionless. To understand this, one should note that

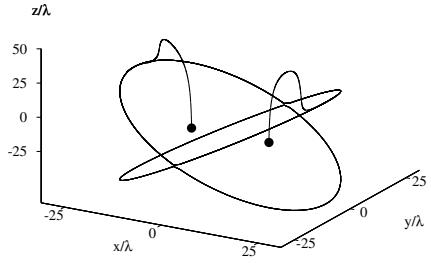

FIG. 10: Trajectories of two Mg^+ ions with different initial locations subject to a two-dimensional optical molasses formed by two pairs of counter-propagating twisted beams, with $l_i = 1$ and $p_i = 0$ for $i = 1 - 4$. It is seen that each ion ends up motionless on the locus of lowest potential energy minima corresponding to two oblique orthogonal circles, as explained in the text.

the deepest potential well is four times as deep as that of a single beam, with the potential minima situated along the locus of spatial points defined simultaneously by two equations $x^2 + y^2 = w_0^2/2$ and $y^2 + z^2 = {w'}_0^2/2$. For ${w'}_0 = w_0$ these two equations describe two orthogonal oblique circles representing the intersection curves of two cylinders of radii $w_0/\sqrt{2}$. Solving for x and y we have $x = \pm z$ and $y = \pm\sqrt{w_0^2/2 - z^2}$. The locus of spatial points where the dipole potential is minimum can be described by the parametric equations $x(u) = (w_0'/\sqrt{2})\cos u$; $y(u) = (w_0'/\sqrt{2})\sin u$; $z(u) = \pm\sqrt{w_0^2/2 - ({w'}_0^2/2)\sin^2 u}$. All Mg^+ ions in the two-dimensional configuration of orthogonal counter-propagating pairs of twisted beams will be trapped at points lying on one of the two oblique circles, as determined by the initial conditions. An ensemble of Mg^+ ions with a distribution of initial positions and velocities will populate the two circles, producing two orthogonal essentially static Mg^+ ion loops. Associated with this system of charges would be a Coulomb field whose spatial distribution, for example, for ions uniformly distributed in the ring can easily be evaluated. When the values of l are such that each pair of beams generates a torque, the motion becomes more complicated, but the ions will seek to congregate in the region of potential minima, while responding to the combined effects of two orthogonal torques and orthogonal axial cooling forces.

When a third pair of counter-propagating beams

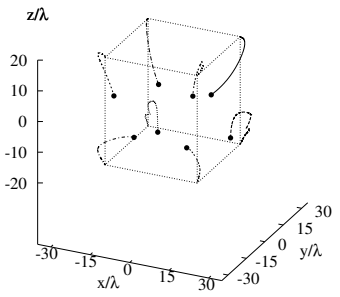

FIG. 11: Trajectories of eight Mg^+ ions in a three-dimensional twisted optical molasses formed by three pairs of counter-propagating Laguerre-Gaussian beams with $l_i = 1$ and $p_i = 0$ where $i = 1 - 8$. The initial velocity of each of the ions is $v_z = 5$ ms^{-1}. The ions end up motionless at the corners of a cube of side w_0.

is added to the two-dimensional configuration, orthogonal to the plane containing the original beams, we have a three-dimensional configuration. In this case the deepest potential minima are located at eight discrete points defined by the coordinates: $x = \pm\frac{w_0}{2}$, $y = \pm\frac{w_0}{2}$, $z = \pm\frac{w_0}{2}$. These coincide with the eight corners of a cube of side w_0, centred at the origin of coordinates, as shown in Fig.11.

7. Rotational effects on liquid crystals

As observed earlier, a liquid crystal is another physical system where new physical effects should arise when subject to twisted light. The most prominent effect in this case can be expected to be an optical influence on the angular distribution of the director $\hat{\mathbf{n}}(\mathbf{r})$ in the illuminated region. To focus on a case of direct and practical relevance, let us consider a liquid crystal film of thickness d occupying the region $0 \leq z \leq d$, with the light incident in such a manner that the beam waist coincides with the plane $z = 0$.

To begin with, we first note that in the absence of the light, the free energy density of the system is given by [53]

$$\mathcal{F}_0(\mathbf{r}) = \frac{1}{2}\mathcal{K}_1 \left[\boldsymbol{\nabla}.\hat{\mathbf{n}}(\mathbf{r})\right]^2 + \frac{1}{2}\mathcal{K}_2 \left[\hat{\mathbf{n}}.\boldsymbol{\nabla}\times\hat{\mathbf{n}}(\mathbf{r})\right]^2 + \frac{1}{2}\mathcal{K}_3 \left[\hat{\mathbf{n}}\times\boldsymbol{\nabla}\times\hat{\mathbf{n}}(\mathbf{r})\right]^2 \quad (44)$$

where $\mathcal{K}_{1,2,3}$ are the Frank elastic constants and the terms represent splay, twist and bend contributions to the free energy density, respectively. As an approximation we set $\mathcal{K}_1 = \mathcal{K}_2 = \mathcal{K}_3 = \mathcal{K}$, corresponding to elastic isotropy. Then Eq.(44) becomes

$$\mathcal{F}_0(\mathbf{r}) = \frac{1}{2}\mathcal{K}\left\{\left[\boldsymbol{\nabla}.\hat{\mathbf{n}}(\mathbf{r})\right]^2 + \left[\boldsymbol{\nabla}\times\hat{\mathbf{n}}(\mathbf{r})\right]^2\right\} \quad (45)$$

Symmetry considerations suggest that $\hat{\mathbf{n}}$ can be written in terms of $\Psi(\mathbf{r})$, the local azimuthal angle such that $\hat{\mathbf{n}} = (\sin\Psi, \cos\Psi, 0)$. The free energy expression thus reduces to

$$\mathcal{F}_0 = \frac{1}{2}\mathcal{K}\boldsymbol{\nabla}\Psi.\boldsymbol{\nabla}\Psi \quad (46)$$

Next consider the electric field of a twisted light beam, at a general position vector $\mathbf{r} = (r, \phi, z)$ in cylindrical coordinates, expressible as

$$\mathbf{E}_{klp}(\mathbf{r}) = \mathbf{f}_{klp}(\mathbf{r})\; e^{i\Theta_{klp}(\mathbf{r})} \quad (47)$$

where $\mathbf{f}_{klp}$ is the electric field amplitude function corresponding to the expressions given in Eq.(7). At frequencies far removed from a molecular resonance, the coupling of the light can be cast in terms of the dielectric properties of the liquid crystal. Ignoring any frequency dispersion, the application of the twisted light thus leads to an additional field-dependent free energy term $\mathcal{F}_{int}$ given by [48]

$$\mathcal{F}_{int} = -\frac{1}{4}\varepsilon_0\varepsilon_a \left(\hat{\boldsymbol{n}}.\boldsymbol{E}_{klp}\right)\left(\hat{\boldsymbol{n}}.\boldsymbol{E}^*_{klp}\right) \quad (48)$$

where ε_a is is the dielectric isotropy of the liquid crystal. Assuming that the field is plane-polarised along the x-axis, we find that total free energy can be written as

$$\mathcal{F} = \mathcal{F}_0 + \mathcal{F}_{int} = \frac{1}{2}\mathcal{K}\boldsymbol{\nabla}\Psi.\boldsymbol{\nabla}\Psi - \Lambda_{klp}\sin^2\Psi(r,z) \quad (49)$$

where $\Lambda_{l,p}$ is given by

$$\Lambda_{klp} = \frac{1}{2}\varepsilon_0\varepsilon_a \left|\mathbf{f}_{klp}\right|^2 \quad (50)$$

Using Landau's free energy formalism, it emerges that Ψ satisfies a second order partial differential equation in two-dimensions (r, z);

$$\mathcal{K}\left\{\frac{\partial^2\Psi}{\partial r^2} + \frac{1}{r}\frac{\partial\Psi}{\partial r} + \frac{\partial^2\Psi}{\partial z^2}\right\} - \Lambda_{l,p}\sin 2\Psi(r,z) = 0 \quad (51)$$

The above theory has been applied to the case of the nematic liquid crystal 5CB (pentylcyanotrphenyl) doped with an anthraquinone derivative

dye (AD1). The system is modelled as an infinitely wide film of thickness d, sandwiched between two thin glass plates, which fix the director angle along the top $z = d$ and bottom $z = 0$. The general boundary conditions are then in the form

$$\begin{aligned} \Psi(r,0) &= \Psi_0 \\ \Psi(r,d) &= \Psi_d \end{aligned} \tag{52}$$

and

$$\left.\frac{\partial \Psi(r,z)}{\partial r}\right|_{r=\infty} = 0 \tag{53}$$

The relevant parameters in this case are $K = 0.64 \times 10^{-12}$ N, and $\varepsilon_a = 0.5832$ [54]. The thickness of the film is taken as $d = 2000\lambda$ where $\lambda = 600$ nm is the wavelength and the intensity of the light is 10^8 Wm^{-2}; the beam waist is taken as $w_0 = 50\lambda$. We consider the cases of $(l,p) = (5,0)$ and $(l,p) = (5,1)$, but the theory can be applied to any l,p mode and we shall choose other modes for illustration.

Figures 12 and 13 display a vector field distribution and the corresponding colour-coded plot of the director orientations in the $r-z$ plane with the boundary conditions $\Psi_0 = 0$ and $\Psi_d = \pi/2$ corresponding to the situation in the absence of the twisted light. Figures 14 and 15 show the

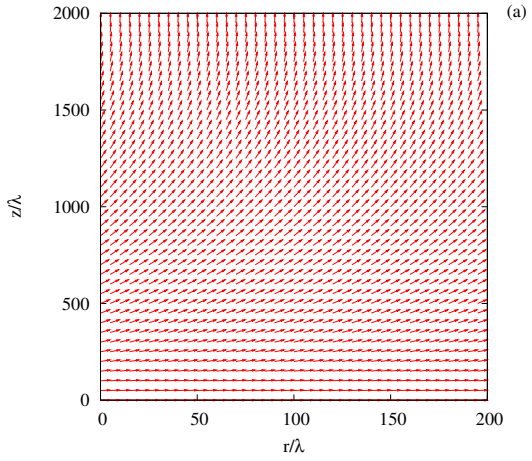

FIG. 12: A vector field representation of the director orientation of the twisted nematic liquid crystal before application of the twisted light. The orientation at the boundaries $z = 0$ (bottom) and $z = d$ (top) are fixed as described in the text.

modified landscape once a twisted light beam with $l = 5, p = 0$ has been switched on. It is clear that

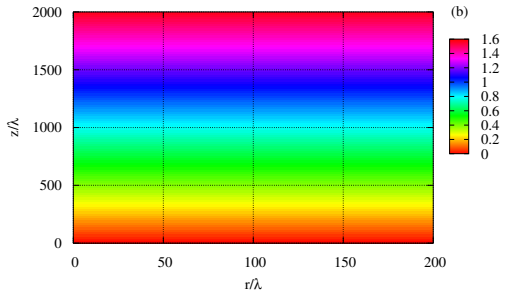

FIG. 13: A colour-coded contour representation of the same data as in Fig. 10. The key represents a scale of the local director orientation angle Ψ relative to the $r-$axis. It spans the angular range $\Psi = 0$ at the bottom (red) to $\Psi = \pi/2$ at the top (magenta)

there is a marked re-orientation of the directors, when compared to the situation in the beam-free case. Figures 16 and 17 concern the case where

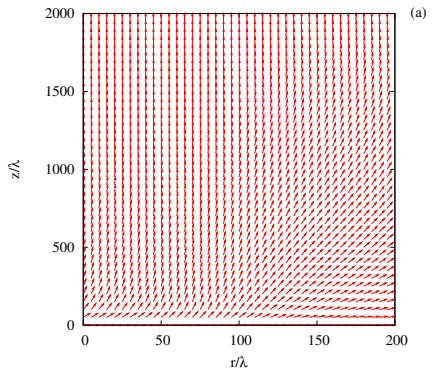

FIG. 14: A vector field representation of the director orientation of the twisted nematic liquid crystal after the application of the twisted LG$_{l,p}$ light where $l = 5, p = 0$

$l = 5, p = 1$ for the applied twisted light mode. It is seen that the differences in the variation of intensity of the light manifest themselves in the director re-orientation.

8. Comments and conclusions

This article has been concerned primarily with a theory of two-level systems responding to the field

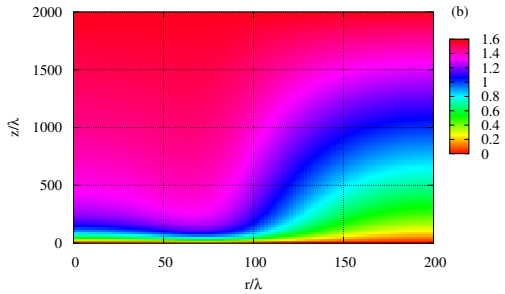

FIG. 15: A colour-coded contour representation of the same data as in Fig. 14. The key represents a scale of the local director orientation angle Ψ relative to the $r-$axis. It spans the angular range $\Psi = 0$ at the bottom (red) to $\Psi = \pi/2$ at the top (magenta)

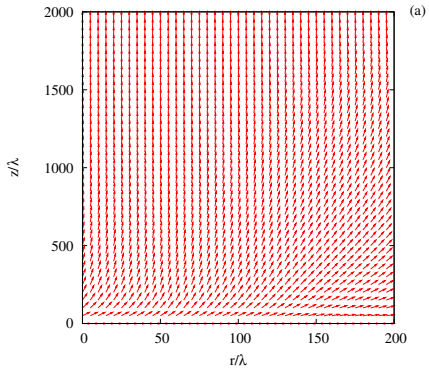

FIG. 16: A vector field representation of the director orientation of the twisted nematic liquid crystal after the application of the twisted $\mathrm{LG}_{l,p}$ with $l = 5, p = 1$. Other parameters are described in the text.

of Laguerre-Gaussian light and, as a supplementary topic, the influence of such light on liquid crystals. The primary aim has been to present an up-to-date account of work in this branch of optical angular momentum effects. The results for atomic, ionic and molecular motion display novel features; not only do such particles experience modified translational forces in such fields, but the radiation forces include rotational components which are solely attributable to to the OAM of the light. In the transient regime, applicable within the time interval of the order of Γ^{-1}, where Γ is the transition rate from the upper state, the particles experience time-dependent forces and torques leading to characteristic particle

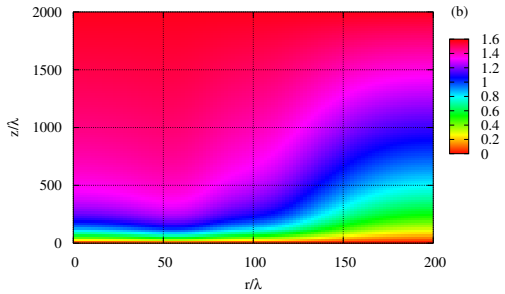

FIG. 17: A colour-coded contour representation of the same data as in Fig. 16. The key represents a scale of the local director orientation angle Ψ relative to the $r-$axis. It spans the angular range $\Psi = 0$ at the bottom (red) to $\Psi = \pi/2$ at the top (magenta).

trajectories. In the steady state regime, applicable for times much larger than Γ^{-1}, the particles experience time-independent forces and torques and the motion leads to cooling, trapping and novel rotational effects in a variety of situations. The saturation light-induced torque has the simple form

$$\boldsymbol{\mathcal{T}} \approx \hbar l \Gamma \hat{\boldsymbol{z}} \tag{54}$$

The result has the simple interpretation that a single transition transfers angular momentum of magnitude $\hbar l$, and since there are Γ transitions per unit time, the product amounts to a torque of magnitude $\hbar \Gamma l$ along the beam axis $\hat{\boldsymbol{z}}$. This supports the prediction that the orbital angular momentum of light is quantised in units of $\hbar$. We have also seen that the two-level system subject to such light experiences a new Doppler shift associated with the rotational component of the interaction. We have seen that this additional Doppler shift is the source of modification of the dissipative forces responsible for laser cooling. The treatments of optical molasses involving pairs of Laguerre-Gaussian beams in one-, two- and three dimensions involve a variety of steady state optical forces with the propensity to produce a novel and highly distinctive behaviour. The Laguerre-Gaussian light generates optical potential wells associated with the total dipole force contributions from all the beams present, while the total dissipative force provides a mechanism for cooling or heating the azimuthal motion along with the axial motion. For each pair of counter-propagating beams, the light-induced torque is doubled or annulled, depending on the relative sign of the OAM quantum number l.

It is clear that the subject of atomic and molecular manipulation using structured light, especially light carrying orbital angular momentum is still at an early stage of development. Experimental work in which atoms, ions and molecules are trapped in optical potentials generated by multiple beams is still to be carried out. Although the theoretical predictions presented here involve trapping in the maximum intensity regions, similar predictions, albeit differing in detail, can be made for trapping in the dark regions of higher order intersecting multiple beams. Moreover, for particles trapped in optical beam arrays, it is also emerging that the light can itself engage with the inter-particle forces. This can, for example lead to azimuthally periodic force fields, generating necklace-like ring structures. In all these potentialities, the exploratory studies conducted so far are giving every indication that there is indeed a rich scope for further technical advances leading to widespread optomechanical applications of structured light [55].

Acknowledgments

The research described in this chapter owes much to work with a number of colleagues and research students, including Les Allen, Vassilis Lembessis, Wei Lai, William Power, Luciana Dávila Romero, Andrew Carter, Mohammad Al-Amri, Simon Horsley and Matt Probert. The authors wish to acknowledge their valuable contributions. Financial support from the Science and Engineering Research Council (EPSRC) are gratefully acknowledged.

References

[1] A. Ashkin, Phys. Rev. Lett. **25**,1321 (1970)
[2] D. G. Grier, Nature **424**, 810 (2003).
[3] See the special journal issue on optical tweezers, J. Mod. Opt. **50**, 1501ff (2003).
[4] K. Dholakia, and P. Reece, Nanotoday, **1**, 19 (2006).
[5] V. S. Letokhov, and V. G. Minogin, *Laser Light Pressure on Atoms* (Gordon and Breach: NY, 1987).
[6] A. P. Kazantsev, G. I. Surdutovich, and V. P. Yakovlev, *Mechanical Action of Light on Atoms* (World Scientific: Singapore, 1990).
[7] C. S. Adams, and E. Riis, Prog. Quant. Electr. **21**, 1 (1997).
[8] C. N. Cohen-Tannudji, Rev. Mod. Phys. **70**, 707 (1998).
[9] C. E. Weiman, D. E. Pritchard, and D. J. Weinland, Rev. Mod. Phys. **71**, S253 (1999).
[10] C. J. Pethick, and H. Smith, *Bose-Einstein Condensation in dilute gases* (Cambridge UP, 2002).
[11] D.L. Andrews, A.R. Carter, M. Babiker, and M. Al-Amri, Proc. SPIE **6131** (2006).
[12] L.C. Dávila Romero, A.R. Carter, M. Babiker, and D.L. Andrews, Proc. SPIE **5736**, 150 (2005).
[13] A. R. Carter, M. Babiker, M. Al-Amri, and D. L. Andrews, Phys. Rev. **A72**, 043307 (2005).
[14] D.L. Andrews, A.C. Carter, M. Babiker, and M. Al-Amri, Proc. SPIE **6131**, 101 (2006).
[15] A. R. Carter, M. Babiker, M. Al-Amri, and D. L. Andrews, Phys. Rev. **A73**, 021401 (2006).
[16] K Volke-Sepolveda, V. Garces-Chavez, S. Chavez-Cerda, J. Arlt, and K. Dholakia, J. Opt. B: Quantum Semiclass. Opt. **4**, S82 (2002).
[17] D. McGloin and K. Dholakia, Contemporary Physics, **46**, 15 (2005).
[18] C. Lopez-Mariscal, J. C. Gottierrez-Vega, G. Milne, and K. Dholakia, Optics Express **14**, 4182 (2006).
[19] A. R. Carter, L. C. Dávila Romero, M. Babiker, D. L. Andrews, and M. I. J. Probert, J. Phys. B-At. Mol. Opt. Phys. **39**, S523 (2006).
[20] R. A. Beth, Phys. Rev. **50**, 115 (1936)
[21] P. J. Allen, Am J. Phys. **34**, 1185 (1966)
[22] R. Simon, and H. J. Kimble and E. C. G. Sudershan, Phys. Rev. Lett. **61**, 19 (1988)
[23] F. Bretenaker and A. Le Floch, Phys. Rev. Lett. **65**, 2316 (1990).
[24] L. Allen, M. W. Beijesbergen, R. J. C. Spreeuw, and J. P. Woerdman, Phys. Rev. A **45**, 8185 (1992).
[25] M. Babiker, W. L. Power, and L. Allen, Phys. Rev. Lett. **73**, 1239 (1994).
[26] L. Allen, M. Babiker, and W. L. Power, Opt. Commun. **112**, 141 (1994).
[27] L. Allen, M. Babiker, W. K. Lai, and V. E. Lembessis, Phys. Rev. A **54**, 4259 (1996).
[28] L. Allen, V. E. Lembessis, and M. Babiker, Phys. Rev. **A53** R2937 (1996).
[29] V. E. Lembessis, Opt. Commun. **159**, 243 (1999).
[30] E. Courtade, O. Houde, J-F Cle'ment, P. Verkerk, and D. Hennequin, Phys. Rev. **A74**, 031403 (2006).
[31] S. J. van Enk, Quant. Opt. **6**, 445 (1994).
[32] M. Babiker, C. R. Bennett, D. L. Andrews, and L. C. Dávila Romero, Phys. Rev. Lett. **89**, 143601 (2002).
[33] G. Juzeliunas, and P. Öhberg, Phys. Rev. Lett. **93**, 033602 (2004).
[34] G. Juzeliunas, P. Öhberg, J. Ruseckas, and A. Klein, Phys. Rev. **A71**, 053614 (2005)
[35] D. M. Villeneuve, S. A. Asyev, P. Dietrich, M.

Spanner, M. Yu Ivanov, and P. B. Korkum, Phys. Rev. Lett. **85**, 542 (2000).
[36] A. Muthukrishnan, and C. R. Stroud Jr., J. Opt. Quantum Semiclass. **4**, S73 (2002).
[37] M. S. Bigelow, P. Zernom, and R. W. Boyd, Phys. Rev. Lett. **92**, 083902 (2004).
[38] A. V. Bezverbny, V. G. Niz'ev, and A. M. Tomaikin, Quantum Electron **34**, 685 (2004).
[39] A. Alexanderscu, E. De Fabrizio, and D. Kojoc, J. Opt. **B7**, 87 (2005).
[40] W. Zheng-Ling, and Y. Jiang-Ping, Chin. Phys. Lett. **22**, 1386 (2005).
[41] J. W. R. Tobosa, and D. V. Petrov, Phys. Rev. Lett. **83**, 4967 (1999).
[42] M. S. Bigelow, P. Zernom, and R. W. Boyd, Phys. Rev. Lett. **92**, 083902 (2004).
[43] S. Al-Awfi, and M. Babiker, J. Mod. Opt. **48**, 847 (2001).
[44] M. A. Clifford, J. Arlt, J. Courtial, and K. Dholakia, Opt. Comm. **156** 300 (1998).
[45] Y. Song, D. Millam, and W. T. Hill III, Opt. Lett. **24**, 1805 (1999).
[46] S. Al-Awfi, and M. Babiker, J. Mod. Opt. **48**, 847 (2001).
[47] T. A. Wood, H. F. Gleeson, M. R. Dickinson, and A. J. Wright, Appl. Phys. Lett. **84**, 4292 (2004).
[48] D. P. Rhodes, D. M. Gherardi, J. Livesey, D. McGloin, H. Melville, T. Freegarde, and K. Dholakia, J. Mod. Opt. **53**, 547 (2006).
[49] P. Domokos, and H. Ritsch, JOSA **B20**, 1098 (2007).
[50] B. Piccirillo, C. Toscano, F. Vetrano, and E. Santamento, Phys. Rev. Lett. **86**, 2285 (2001).
[51] B. Piccirillo, A. Vella, and E. Santamento, J. Opt. **B4**, S20 (2004).
[52] M. V. Berry, in Proceedings of the meeting in singular optics, Frunzenskoe, Crimea (1988), SPIE Proceedings, **3487** (1988).
[53] I. W. Stewart *The static and dynamic continuum theory of liquid crystals* (London: Taylor and Fransis, 2004).
[54] D. O. Krimer, G. Demeter, and L. Kramer, Phys. Rev. E **66**, 031707 (2002).
[55] D. S. Bradshaw, and D. L. Andrews, Opt. Lett. **30**, 3039 (2005).

Received: 17 July, 2007
Accepted: 28 July, 2007